Dalton Transactions

Accepted Manuscript

This is an *Accepted Manuscript*, which has been through the Royal Society of Chemistry peer review process and has been accepted for publication.

Accepted Manuscripts are published online shortly after acceptance, before technical editing, formatting and proof reading. Using this free service, authors can make their results available to the community, in citable form, before we publish the edited article. We will replace this *Accepted Manuscript* with the edited and formatted *Advance Article* as soon as it is available.

You can find more information about *Accepted Manuscripts* in the Information for Authors.

Please note that technical editing may introduce minor changes to the text and/or graphics, which may alter content. The journal's standard Terms & Conditions and the Ethical guidelines still apply. In no event shall the Royal Society of Chemistry be held responsible for any errors or omissions in this *Accepted Manuscript* or any consequences arising from the use of any information it contains.

ROYAL SOCIETY OF CHEMISTRY

www.rsc.org/dalton

Please do not adjust margins

Journal Name

ARTICLE

Supramolecular Fluorescence Enhancement via Coordination-Driven Self-Assembly in Rigid bis-Picolylcalixarene-derived Blue-Emitting $M_2L_2X_n$ Macrocycles†

Received 00th January 20xx,
Accepted 00th January 20xx

DOI: 10.1039/x0xx00000x

www.rsc.org/

Edmundo Guzmán-Percástegui,[a] Mireille Vonlanthen,[b] Beatriz Quiroz-García,[a] Marcos Flores-Alamo,[c] Ernesto Rivera[b] and Ivan Castillo*[a]

The lower-rim functionalised distal bis-(4-picolyl)-*p-tert*-butylcalix[4]arene (**L**) selectively and quantitatively self-assembles into a series of discrete [2+2] blue-emitting metallacycles of general formula $\mathbf{M_2L_2X_n}$ with diverse metal salts (M = Zn^{2+}, Pd^{2+}, Ag^{+}, and Cd^{2+}; X = Cl^{-}, NO_3^{-}, ClO_4^{-}, BF_4^{-}, $CF_3SO_3^{-}$, PF_6^{-}, SbF_6^{-}; n = 2, 4). Macrocycle assembly has been corroborated by 2D-DOSY NMR and ESI-MS analyses, which further indicate that the $\mathbf{M_2L_2X_n}$ entities are quite stable and persist as robust and discrete macrocyclic species in solution. While free **L** units display modest blue emission (λ_{max} = 307–405 nm), self-assembly of $\mathbf{M_2L_2X_n}$ results in amplified fluorescence (up to 13-fold). This remarkable enhancement may be primarily ascribed to the increase in conformational rigidity imposed on the **L** units by supramolecular assembly formation upon metal coordination to the pyridyl groups; in addition, subtle intesity-emission modulation may be provided by the different metal components. Titrations aimed at exploring the possibilities for ratiometric detection of metal cations or sensing of nitroaromatic species, revealed that the $\mathbf{M_2L_2X_n}$ platform may be a suitable "turn-on/off" system. Our results provide valuable insights into luminescence enhancement within the context of coordination-driven assemblies, which may be engineered to increase their fluorescence by imposing rigidity on the chromophores.

Introduction

Coordination-Driven Self-Assembly is an effective and versatile strategy to design and construct aesthetically appealing 2D and 3D metallo-structures by judicious combination of donor and acceptor components of suitable geometries.[1,2] The low synthetic cost and the usual outcome of a single thermodynamic product under mild conditions, not only makes available tailor-made assemblies of desired shape and size, but also promises direct access to advanced multifunctional supramolecular coordination complexes in high yields.[3] The past few years in particular have witnessed a tremendous progress in the engineering of photoactive coordination-driven architectures with perspectives in molecular sensing, cell imaging, and materials science.[4,5] Despite continuous advances in these areas, it is not yet possible to fully control the luminescent response of supramolecular entities; in this sense, the ability to alter photophysical properties through rational structural modifications becomes of utmost relevance. Of special interest are the factors directly related to self-assembly, which may induce higher emission of photoactive assemblies. In practice, fluorescence enhancement by supramolecular coordination complex formation is generally achieved by blocking the PET quenching (Photoinduced Electron Transfer),[6] or by the sensing of various chemical species.[7] In search of easily-accessible modular systems with tunable optical elements, we examined the repercussions of self-assembly on the modestly emissive bis-(4-picolyl)-*p-tert*-butylcalix[4]arene **L**, affording a series of blue-emissive $\mathbf{M_2L_2X_n}$ metallamacrocycles with a variety of metals (Scheme 1). The semi-flexible tecton **L** was employed to control the shape, size, and stoichiometry of this new class of supermolecules. We envisaged that the orientation of the 4-picolyl moieties as adaptable and flexible coordination sites, would direct the construction of discrete macrocycles over potential oligomeric or polymeric species. Although calix[4]arenes represent one of the most iconic classes of macrocyclic motifs in supramolecular chemistry,[8] they have been seldom employed in multi-metal self-assembly. Sophisticated examples include architectures covalently assembled through carboxylic[9] and dithiocarbamate[10] functionalities, as well as metal clusters.[11] Surprisingly, little work has been reported on coordination-

[a] *Instituto de Química, Universidad Nacional Autónoma de México, Circuito Exterior, Ciudad Universitaria, México D.F. 04510, México.*
[b] *Instituto de Investigaciones en Materiales, Universidad Nacional Autónoma de México, Circuito Exterior, Ciudad Universitaria, México D.F. 04510, México.*
[c] *Facultad de Química, Universidad Nacional Autónoma de México, Ciudad Universitaria, México D. F. 04510, México.*

†Electronic Supplementary Information (ESI) available: Detailed synthetic procedures of macrocycles **1-10**, IR, ^{1}H NMR, 2D-DOSY NMR, ESI-MS, UV-Vis, emission data, additional information regarding fluorescence-on/off titrations, and crystallographic information of **L** are provided. See DOI: 10.1039/x0xx00000x

Dalton Transactions Accepted Manuscript

driven calixarene complexes,[12] with a single example regarding a crystal structure of a coordination macrocycle.[13] Moreover, investigations on photoactive coordination-driven calixarene assemblies are virtually non-existent. Thus, we herein present an investigation of the impact of self-assembly on the fluorescence of calixarene **L**, providing a first glimpse into the potential of this class of macrocycles as turn-on/off prototypes for cation and nitroaromatic sensing. To the best of our knowledge, this work represents the first example of a novel family of photoactive self-assembled coordination macrocycles based on a calix[4]arene derivative, typifying the luminescent enhancement in terms of the increase of molecular rigidity in $\mathbf{M_2L_2X_n}$ systems. While supramolecular rigidity has been envisaged as a factor for improving fluorescence of coordination-driven assemblies,[5,14] reports in this area are seldom encountered. We herein present a unique platform to examine the role of conformational constraint upon self-assembly, which may have been overlooked in early supramolecular coordination design, thus providing advantageous insights into principles of luminescence tuning.

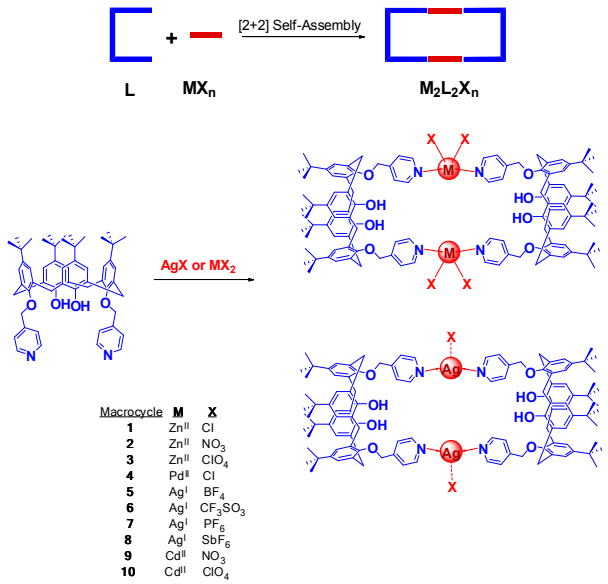

Macrocycle	M	X
1	Zn^{II}	Cl
2	Zn^{II}	NO_3
3	Zn^{II}	ClO_4
4	Pd^{II}	Cl
5	Ag^{I}	BF_4
6	Ag^{I}	CF_3SO_3
7	Ag^{I}	PF_6
8	Ag^{I}	SbF_6
9	Cd^{II}	NO_3
10	Cd^{II}	ClO_4

Scheme 1 General synthesis of metallomacrocycles **1–10**.

Results and Discussion

Synthesis and Characterisation of $M_2L_2X_n$ Metallomacrocycles

Initially, the solid-state structure of calixarene **L** was determined by X-ray crystallography. Single crystals were obtained in the triclinic space group $P\bar{1}$ by slow evaporation of a concentrated dmso solution (see ESI†). The asymmetric unit consists of one molecule of calix[4]arene **L** as well as two disordered molecules of dmso. The molecular structure of **L** confirms the presence of two picolyl groups at distal position on the lower rim of the macrocycle, as well as a cone conformation (characterised by intramolecular O–H···O hydrogen bonding) adopted by the calix[4]arene. An ORTEP representation of **L** is depicted in Fig. 1.

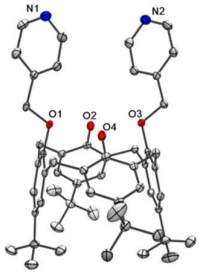

Fig. 1 ORTEP representation of calixarene **L** (50% thermal elipsoids). Disordered DMSO solvent molecules and hydrogen atoms have been omitted for clarity.

The preparation of dinuclear $\mathbf{M_2L_2X_n}$ macrocycles was achieved by mixing the corresponding M^{n+} salt (M = Ag^+, Pd^{2+}, Zn^{2+}, and Cd^{2+}) with **L** in 1:1 ratio under mild conditions. It was anticipated that the orientation of the N-donors at the 4-positions (angle between lone pairs close to 0°, Fig. 1) would lead to selective [2+2] self-assembly of macrocycles as thermodynamic products, in contrast to the previously reported mononuclear or polymeric complexes obtained with 2-picolyl groups in the presence of Cu^{2+} ions.[15] Initial reactions between **L** and $M(NO_3)_2$ (M = Zn^{2+}, Cd^{2+}) in a 1:1 ratio in $CHCl_3$ or CH_2Cl_2 led to complex mixtures as determined by ^{1}H NMR spectroscopy, suggesting the presence of the desired macrocycles and oligomeric species. The use of more polar solvents such as MeOH or CH_3CN allowed the isolation of microcrystals formulated as the desired macrocycles in nearly quantitative yields. The simplicity of this methodology illustrates the level of control provided by the coordination-driven self-assembly approach,[16] suggesting that the main driving force for the selective association into macrocycles may be the hydrophobicity of **L**.

The ^{1}H NMR spectrum of **L** displays one set of signals for each half of the molecule that remains unchanged upon $\mathbf{M_2L_2X_n}$ assembly, indicative of the presence of a single C_2-symmetric species. Additionally, all $\mathbf{M_2L_2X_n}$ ^{1}H NMR spectra display a pair of doublets ranging from 3.3 to 4.3 ppm assigned to the typical AB spin system of the bridging $-CH_2-$ groups of calixarene units, indicating that cone conformation of **L** is preserved upon macrocycle formation in all cases. The chemical shifts of the pyridyl protons Ha_{py} and Hb_{py} are highly sensitive towards metal ion coordination, with significant downfield shifts due to deprotection upon cation binding (Fig. 2). While this represents the most evident feature in the ^{1}H NMR spectra of the macrocycles, the remaining resonances are only slightly affected by coordination. Furthermore, the ^{1}H NMR spectra of the macrocycles bearing Pd^{2+} and Ag^+ ions display sharp signals indicating free motion, consistent with the anticipated rectangular macrocyclic shapes given the coordination preferences of Ag^+ and *trans*-disubstituted Pd^{2+} ions. In contrast, in the spectra of Zn^{2+} and Cd^{2+} metallomacrocycles the signals tend to broaden, possibly due to the more restricted motion imposed by the tetrahedral environment around Zn^{2+} and Cd^{2+} centres that give rise to "twisted"

Dalton Transactions Accepted Manuscript

This journal is © The Royal Society of Chemistry 20xx

Please do not adjust margins

macrocycles, as predicted by Merck Molecular Force Field (MMFF) simulations (*vide infra*). It is noteworthy that this effect is more pronounced in the case of Cd^{2+} complex **10**, where the doublets assigned to H*a* and H*b* are split into an additional pair of broad doublets; this may be attributed to the more hindered rotation of the pyridine rings upon coordination to bulky cadmium perchlorate motifs.

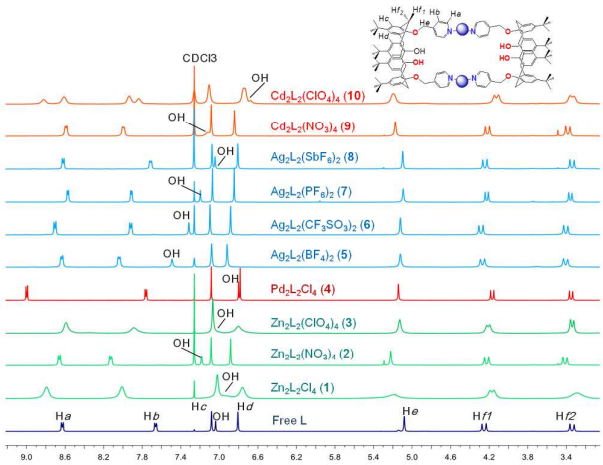

Fig. 2 Partial ^{1}H NMR spectra of **L** and $\mathbf{M_2L_2X_n}$ macrocycles **1–10** in $CDCl_3$ at 25°C.

Diffusion-ordered NMR spectroscopy (DOSY) spectra showed that all proton resonances of the complexes exhibit the same diffusion coefficient (see ESI†); accordingly, the selective formation of a single assembly is confirmed. By applying the Stokes-Einstein equation, we estimated the hydrodynamic radii (*r*H) of different metallomacrocycles, diffusion coefficients and calculated radii are given in Table 1. The *r*H values of the assemblies are nearly double the value determined for **L**, providing strong evidence for the larger dimensions of the metallic species, which are in reasonable agreement with the $\mathbf{M_2L_2X_n}$ formulation and indicate that these macrocycles persist in solution as discrete dinuclear species. Likewise, the formation of higher order assemblies, such as coordination oligomers or smaller 1:1 $\mathbf{MLX_n}$ complexes is ruled out. It is worth mentioning that in all cases the *r*H values represent average molecular sizes, which may involve the potential effect of counterions and the nearest solvation shell, especially for Zn^{2+} and Cd^{2+} macrocycles. Perhaps more importantly, the diverse macrocycle conformations arising from the varied coordination geometries should also account for variations in size among the series of macrocycles prepared. For instance, the smaller *r*H values observed for the Ag^+ metallomacrocycles (from 9.0 to 10.0 Å) may arise from the presence of only one counterion for each silver centre and a roughly rectangular macrocycle shape.

Table 1. Measured diffusion constants and calculated hydrodynamic radii for **L** and **1–10** as $CDCl_3$ solutions at 298 K.

Compound	Diffusion Coefficients ($\times 10^{-10}$ m^2/s, 298 K)	Hydrodynamic radii *r*H (Å)
Free **L**	5.83	6.88
1 $Zn_2L_2Cl_4$	3.63	11.10
2 $Zn_2L_2(NO_3)_4$	3.61	11.25
3 $Zn_2L_2(ClO_4)_4$	3.05	13.20
4 $Pd_2L_2Cl_4$	3.73	10.81
5 $Ag_2L_2(BF_4)_2$	4.46	9.04
6 $Ag_2L_2(CF_3SO_3)_2$	4.16	9.69
7 $Ag_2L_2(PF_6)_2$	4.03	9.97
8 $Ag_2L_2(SbF_6)_2$	4.30	9.37
9 $Cd_2L_2(NO_3)_4$	3.34	12.07
10 $Cd_2L_2(ClO_4)_4$	3.09	13.03

The molecular $\mathbf{M_2L_2X_n}$ (n = 2, 4) composition of [2+2] assemblies was confirmed by ESI-MS analysis (see ESI†). In general, the spectra indicate the exclusive formation of the target macrocycles. Nonetheless, in some cases it is possible to distinguish species of slightly higher molecular weight arising from coordination of solvents or capture of free metal ions; such reactivity may be feasible under ESI-MS conditions (Figures S26 and S28, ESI†). Overall, the spectra showed charged states consistent with the macrocyclic fragments $\mathbf{[M_2L_2X_{n-1}]^+}$ as a result of the loss of one counterion, except for macrocycle **10**, where it was only possible to observe peaks attributable to a proposed hemimacrocycle $\mathbf{[CdL_2(ClO_4)]^+}$; the observed peaks are in good agreement with calculated isotopic distributions. Peaks assignable to generic $\mathbf{[AgL_2]^+}$ and $\mathbf{[ML_2X]^+}$ hemimacrocycles were also detected in most cases, suggesting that a general pathway for disassembly may proceed through such species. Notably, all ESI-MS spectra of silver macrocycles **5–8** exhibit a common pattern displaying peaks consistent with $\mathbf{[AgL_2]^+}$ and $\mathbf{[AgL]^+}$ at approximately *m/z* = 1769 and 939, respectively. Given that DOSY-NMR and ESI-MS techniques constitute suitable means for the solution characterisation of supramolecular assemblies,[17] these data provide compelling evidence of the stability of macrocycles **1–10** in solution, in both nonpolar (CH_2Cl_2, $CHCl_3$) and polar (CH_3OH, CH_3CN) solvents. In addition to the satisfactory DOSY and ESI-MS data, as well as elemental analyses, the target macrocycles were modelled by means of MMFF simulations in order to predict their shape and size. The model structures of palladium complex **4** and silver macrocycles **5–8** feature roughly rectangular shapes, as envisaged given the metal coordination preferences. Meanwhile, simulations of macrocycles containing Zn^{2+} and Cd^{2+} predict a helical-type shape imposed by the expected tetrahedral geometries of these ions. As a result of the twisted macrocyclic conformation, the MMFF models suggest the presence of an inner cavity with potential to host small guests such as solvent molecules or additional metal ions (Fig. 3). In all cases, the values obtained for the diameters from molecular modelling (distance between the two most distant points of calixarene units) were comparable to the calculated diameters from the diffusion coefficient using the Stokes–Einstein equation. These results predict that the

Dalton Transactions Accepted Manuscript

semi-flexible **L** is able to adopt diverse macrocyclic conformations through N_{py}–M bonds, leading to varied conformations in order to meet the geometric requirements of each metal ion. Unfortunately, all efforts to obtain X-ray quality crystals of the macrocycles were unsuccessful; a few well-formed crystals were obtained, but apparently the presence of large voids resulted in weak scattering to collect satisfactory data.

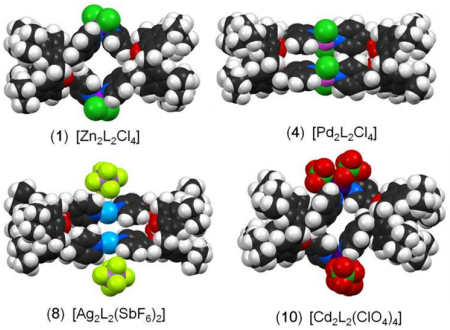

Fig. 3 Proposed space-filling molecular models of macrocycles displaying varied conformations (Spartan, MMFF).

Photophysical Properties of $M_2L_2X_n$ Metallomacrocycles

In order to discern the role of metallomacrocyclic self-assembly in emission modulation, we measured absorption and emission of **L** at twice the concentration of the macrocycles to keep the stoichiometry of the ligand in the supramolecular assemblies. The UV-vis spectra of **L** and macrocycles **1**–**10** in MeOH exhibit a prominent absorption band at λ_{max} = 280 nm assigned to π–π* symmetry-allowed intraligand transitions. The absorption spectra are similar among the whole series, showing that the energy of the bands is not sensitive to the identity of the metal, with only minor changes in absorption coefficients. Upon excitation of MeOH solutions (λ_{ex} = 280 nm), **L** exhibits a single emission band at λ_{max} = 307 nm. Notably, most $\mathbf{M_2L_2X_n}$ macrocycles display a fluorescence enhancement relative to the parent calixarene **L**, with a stronger single emission band around the wavelength observed for **L** (λ_{max} ≈ 307 nm) and no additional emission peaks. All macrocycles afford nearly identical spectra to the uncoordinated **L**, evidencing that the emission can be traced to the calixarene scaffolds, and that self-assembly did not alter the shape of the parent spectrum (Fig. 4). Macrocycles $\mathbf{Ag_2L_2(SbF_6)_2}$ (**8**), $\mathbf{Zn_2L_2(ClO_4)_4}$ (**3**) and $\mathbf{Ag_2L_2(PF_6)_2}$ (**7**) display the highest emission, whereas self-assembly of macrocycles $\mathbf{Zn_2L_2(NO_3)_4}$ (**2**), $\mathbf{Cd_2L_2(NO_3)_4}$ (**9**) induce poor emission, and $\mathbf{Pd_2L_2Cl_4}$ (**5**) even quenches the fluorescence to some extent. Thus, the observed change in fluorescence intensity ranged from 20% to 350% upon self-assembly, as compared to the emission of two uncoordinated **L** tectons in MeOH.

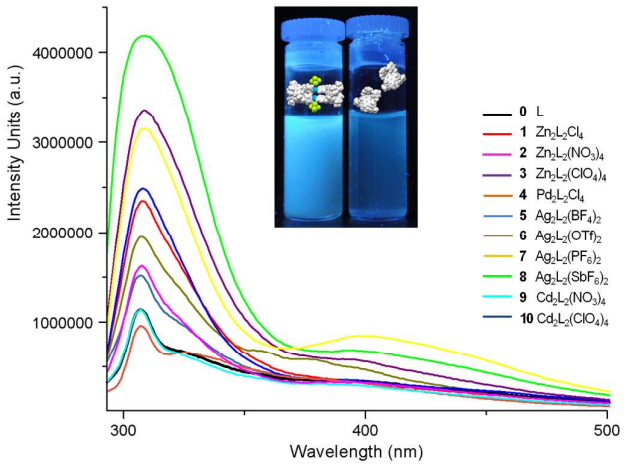

Fig. 4 Fluorescence spectra of **L** (17.0×10^{-6} M) and $\mathbf{M_2L_2X_n}$ (8.5×10^{-6} M) recorded in CH_3OH at room temperature, λ_{ex} = 280 nm. Inset: pictures of emitting solutions of $\mathbf{Ag_2L_2(SbF_6)_2}$ (**8**, *left*), and **L** (**0**, *right*).

We also examined the luminescent behaviour of this family of macrocycles as $CHCl_3$ solutions; excitation at λ_{ex} = 280 nm yielded spectra with a different pattern than that observed in MeOH. The former band at λ_{max} = 307 nm is observed along with more intense peaks (λ_{max} = 354, 373 and 392 ± 4 nm). In contrast, the absorption features do not present a solvatochromic shift, with UV-vis spectra recorded in $CHCl_3$ nearly identical to those determined in methanolic solutions, λ_{max} ≈ 280 nm (Fig. S33, ESI†). For most $\mathbf{M_2L_2X_n}$ macrocycles their emissive properties as $CHCl_3$ solutions can be described as modest. Nevertheless, outstanding exceptions are $\mathbf{Ag_2L_2(SbF_6)_2}$ (**8**) and $\mathbf{Zn_2L_2(ClO_4)_4}$ (**3**), which exhibit 13-fold and 9-fold emission enhancements in the same solvent, respectively; their strongest blue emission is centred at λ_{max} ≈ 375 nm (Fig. 5).

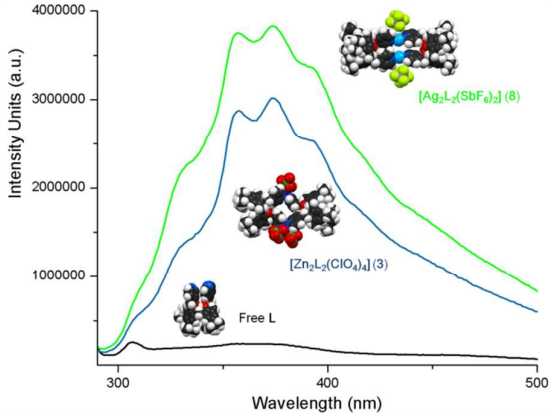

Fig. 5 Macrocycles displaying the highest enhanced emission relative to the parent **L** ligand in $CHCl_3$ (8.5×10^{-6} M for $\mathbf{M_2L_2X_n}$ and 17×10^{-6} M for **L**).

The observations described above attest that supramolecular assembly may yield distinctive and improved photonic functionality relative to the parent isolated luminophores. In our case *two assembled molecules (**L**), locked in the* $\boldsymbol{M_2L_2X_n}$

Dalton Transactions Accepted Manuscript

This journal is © The Royal Society of Chemistry 20xx

Please do not adjust margins

*macrocycles, emit stronger fluorescence than two disassembled **L** molecular entities*. The improved emission of the macrocycles may be primarily ascribed to the increased rigidity of **L** as emissive building blocks upon self-assembly. The flexible picolyl arms are partially locked by formation of four N_{py}–M bonds, with a geometric arrangement that is determined by the specific metal ion involved. While luminescence in the majority of examples of coordination-driven assemblies relies on the intrinsic high photoactive properties of rigid organic building blocks, our results are intriguing for the reason that we achieved improved emissions simply by increasing rigidity as main element upon self-assembly of the relatively flexible and poorly emissive tecton **L**. The conformational restraints seemingly minimise structural perturbations, such as vibrations and torsions associated with non-radiative decay that deactivate the excited state of the pyridine-containing **L** chromophores; as a result, the emission properties due to macrocycle formation are significantly enhanced. Interestingly, similar fluorescence enhancement related to the increase of rigidity and restricted motions has been observed in many molecular systems that do not involve self-assembly.[18] Only in a few very recent examples this increase in rigidity has been proposed to be a factor for the enhanced emission of photoactive ligands upon self-assembly.[5,14] The resulting emission intensity can be further modulated by electronic effects on **L** units induced by each metal component. Cd^{2+} ions, for example, tend to induce poor emission enhancement when compared to Zn^{2+} ions, probably due to the usual quenching effect of heavy-atoms.[19] Likewise, emission of $\mathbf{Ag_2L_2X_2}$ macrocycles **5**–**8** proves that the nature of the counterion is important: generally, all AgX salts (X = BF_4^-, OTf^-, PF_6^-, and SbF_6^-) cause higher emission than **L** in MeOH, with $AgSbF_6$ inducing the highest fluorescence response among the silver salts even in $CHCl_3$. It is worth to point out that the investigation into the role of metal ions in assemblies should be fundamental for the development of novel functional materials, considering that such studies remain relatively scarce.[20]

Metal Ion Sensing in Methanol

Given that **L** exhibits an increase in fluorescence intensity in the presence of the metal ions employed, we performed fluorescence titrations on **L** to monitor self-assembly and to examine the potential for metal ion binding at different stoichiometric ratios. Titrations of **L** with $ZnCl_2$, $Zn(ClO_4)_2$ and $AgSbF_6$ in MeOH were chosen as representative examples. When a 1:1 ratio was attained, and after approximately 1 h at room temperature, fluorescence measurements afforded stable values indicative of exclusive $\mathbf{M_2L_2X_n}$ formation. Under these conditions, a good response to additional Zn^{2+} ions was observed, since fluorescence intensity does not saturate upon formation of the putative macrocycle with $\mathbf{Zn_2L_2X_4}$ stoichiometry when one equivalent of Zn^{2+} relative to **L** is present. For instance, when excess $ZnCl_2$ is added to the *in situ* formed $\mathbf{Zn_2L_2Cl_4}$, macrocycle **1** displays fluorescence enhancement until addition of up to 5 equivalents of $ZnCl_2$ (Fig. S35, ESI†). Likewise, titration of **L** with $Zn(ClO_4)_2$ revealed that addition of 1 equivalent of salt led to an emission enhancement without any spectral changes after approximately 50 minutes, indicating that assembly of macrocycle **3** is complete within this period. In order to determine if ClO_4^- increases emission, this was probed by addition of $NaClO_4$ solutions, but little effect on fluorescence emission was observed (enhancement of 8% with addition of 2 equivalents). In contrast, **3** displayed a continuous turn-on enhancement upon addition of up to 30 equivalents of Zn^{2+} (Fig. 6). Finally, addition of a solution of $AgSbF_6$ to **L** resulted in the highest fluorescence enhancement on **L** obtained with only one equiv of Ag^+, although excess of $AgSbF_6$ still had a slight enhancement effect on the emission spectra (Fig. S36, ESI†).

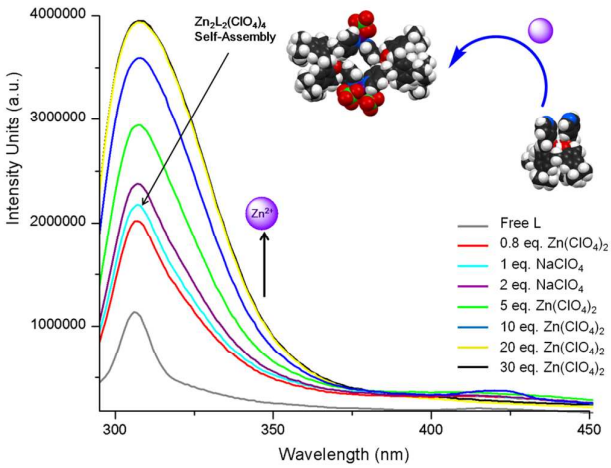

Fig. 6 Enhancement of fluorescence of **L** (8.5×10^{-6} M solution in MeOH) upon assembly of macrocycle $\mathbf{Zn_2L_2(ClO_4)_4}$ (**3**), and relative changes upon addition of excess of $Zn(ClO_4)_2$. Inset: simulation representing the assembly of macrocycle **3**.

Fluorescence titrations of **L** with Zn^{2+} and Ag^+ ions confirm the enhancement of blue emission associated to the formation of the $\mathbf{M_2L_2X_n}$ macrocycles. This illustrates that the coordination-driven self-assembly approach could serve as basis for the development of ion detection systems with "turn-on" signalling, which is often more desirable than "turn-off" metal detection for better selectivity and sensitivity.

Detection of nitroaromatic species

Since fluorescent coordination-driven assemblies have been successfully employed as sensors for diverse nitro-containing explosives via turn-off signaling,[4a,21] we explored the possibility of using macrocycles **1–10** for sensing nitroaromatic compounds by monitoring their blue fluorescence under UV light. In this context, picric acid (PA) has been widely employed as chemical reagent in pharmaceutical, firework and leather-dye industries, resulting in its widespread presence as environmental pollutant with repercussions on human health. Its highly explosive nature makes the development of selective and inexpensive chemosensors for PA a topic of paramount interest for safety and environmental remediation.

Dalton Transactions Accepted Manuscript

In order to illustrate the potential of macrocycles **1–10** as sensors, we investigated the fluorescence response of selected macrocycles **2**, **5**, **8** and **10** towards PA. The initial emission gradually decreased with broadening of the spectrum, while the intense and sharp bands progressively disappeared, accompanied by appearance of a low-energy shoulder at *ca.* 450 nm that may be assigned to the formation of an intermolecular charge transfer complex, as usually assumed for the interaction between PA and the fluorogenic unit.[21,22] This low-energy band was detected after addition of one equivalent of PA. The fluorescence quenching data were also analyzed using the Stern-Volmer equation to obtain an association or quenching constant (K_{ass}); the nonlinear upward curve plot implies in all cases the engagement of a dual static and dynamic mechanism in the fluorescence quenching (Figs. S37, S38, S40, and S41, ESI†). The K_{ass} values and the PA concentrations required to quench emission *ca.* 90% are shown in Table 2. The highest quenching efficiency is observed in **10** among the tested metallacycles; Figs. 7, S39, and S41 show the changes in fluorescence upon addition of PA to **2**, **5**, **8** and **10**. These preliminary results suggest that larger metallacycles bearing tetrahedral metal ions (Zn^{2+} and Cd^{2+}), display higher quenching efficiency than macrocycles assembled through linear Ag^{+} ions; this might be associated to the enforced conformations and the predicted size of each macrocycle based on the corresponding metal ions.

Table 2. Picric Acid (PA) concentration to quench emission of metallacycles **2**, **5**, **8**, and **10**, and K_{ass} (from Stern-Volmer equation).

Macrocycle	PA (μM)[a]	K_{ass} ($\times 10^3$ M^{-1})
$Zn_2L_2(NO_3)_4$ (2)	638	1.52
$Ag_2L_2(BF_4)_2$ (5)	672	1.01
$Ag_2L_2(SbF_6)_2$ (8)	680	1.00
$Cd_2L_2(ClO_4)_4$ (10)	765	1.65

[a] Concentration of PA needed to quench emission *ca.* 90%.

Further insight into the interaction between macrocycles and PA in solution, and proof for strong binding are evidenced by ^{1}H NMR titration studies, with incremental addition of PA inducing changes in the spectral patterns of the tested macrocycles. In general, the NMR spectra are characterised by a gradual broadening of resonances and downfield shifting of the signals corresponding to pyridyl protons H*a* and H*b*, as well as the methylene groups H*e* in the 4-position of the pyridine rings upon addition of PA; the largest downfield shift for this set of signals suggests that the PA···$\mathbf{M_2L_2X_n}$ interaction occurs mainly in the proximity of the picolyl moieties: the H*b* protons experience the largest downfield shift, indicating a major electron withdrawing effect on such protons. Notably, the phenolic –OH protons exhibit a high sensitivity towards the presence of PA, evidenced in the downfield shifts and broadening of the corresponding signals. Interestingly, the addition of PA to macrocycle **10** led to a gradual downfield shifting and sharpening of signals corresponding to the pyridyl rings; the original four-signal pattern (H*a1*, H*a2*, H*b1* and H*b2*, Figs. 2 and 7) is simplified into a pair of sharp doublets, H*a* and H*b*, similar to those observed for **1–9**. Likewise, PA resonances undergo a downfield shift likely associated to the variations in solution from the bound charge-transfer state to the unbound state of PA. This effect has been observed for coordination-driven metallacycles in the presence of PA as quencher.[22] The NMR data strongly indicate interaction between PA and macrocycles, likely via formation of a charge-transfer complex. This interaction is mainly localised in the proximity of the picolyl rings and the free OH groups, given the high sensitivity of these protons to the presence of PA in the NMR spectra. Overall, the examined macrocycles exhibit fast and sensitive fluorescence quenching behaviour towards PA, thus rendering them as a promising family of macrocycles for the detection of nitro-containing explosives. This behaviour will be investigated in detail in forthcoming work.

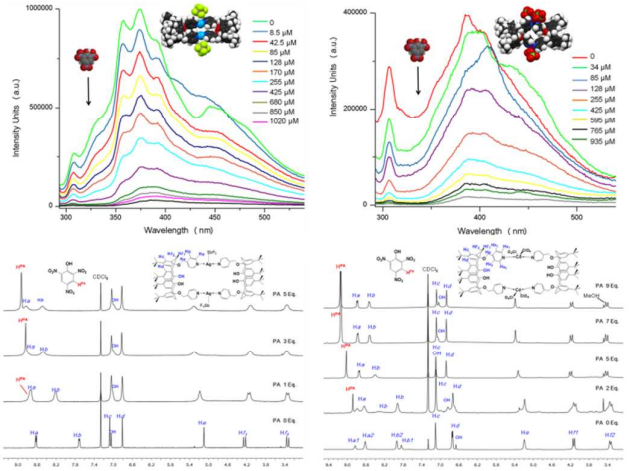

Fig. 7 Fluorescence quenching profiles of $CHCl_3$ solutions (8.5×10^{-6} M) of macrocycles **8** (*left*) and **10** (*right*) upon gradual addition of PA (1.0×10^{-3} M solution in $CHCl_3$) along with the corresponding ^{1}H NMR partial titration plots in $CDCl_3$ at room temperature.

Conclusions

We have presented a rational and simple strategy to afford a novel family of discrete [2+2] metallomacrocycles using a bis-picolylcalix[4]arene derivative with control over stoichiometry and size via the coordination-driven self-assembly approach. These robust macrocycles persist in solution as evidenced by 2D-DOSY NMR and ESI-MS experiments. MMFF simulations predict that calixarene **L** is able to adjust to the variable geometric needs of diverse metals ions that maintain the supramolecular integrity, despite their varied conformational arrangements. Generally, macrocycles **1–10** display stronger emission than the parent **L**, demonstrating that two assembled **L** molecules emit stronger fluorescence than two uncoordinated **L** molecules. Such effect may be primary triggered by the supramolecular rigidity imposed on **L** by the metal ions in the macrocycles, so that the N_{py}–M interactions restrict the molecular motions and minimise non-radiative decay mechanisms. Secondly, the intensity of emission is further modulated according to the electronic properties of the metal centres, while preserving the blue emissive colour.

Dalton Transactions Accepted Manuscript

This journal is © The Royal Society of Chemistry 20xx

The latter property may be further exploited to tune the fluorescence of blue emitting materials, and possibly to develop novel emitters at different wavelengths. Our observations imply that our strategy to assemble macrocycles appears to be promising prototype for chemosensors, with **L** and $\mathbf{M_2L_2X_n}$ as versatile luminescent probes for "turn-on" metal detection or "turn-off" sensing of nitroaromatics, respectively.

The results herein presented should stimulate the use of calixarenes and related supramolecular macrocyclic platforms as versatile scaffolds for photoactive coordination-driven assemblies. This may result in novel sensors with architectures comprising the calixarene cavities, combined with preorganised metal-binding sites. To the best of our knowledge, this is the first report that combines the use of calixarenes in coordination-driven self-assembly with potential applications in emission enhancement, and potential for turn-on/off signaling sensors. This rigidity principle may be extended to the design of new types of photoactive functional materials in the context of architecture-dependent supramolecular sensors by fluorescence enhancement, and also to achieve fine-tuning of fluorescence through the binding of selected metal ions. Further exploration of these types of systems with different metals, solvents, and anions remain to be evaluated for the development of novel fluorescent probes.

Experimental details

Materials and methods

Reagents were purchased from commercial suppliers and used as received. All solvents were purified and distilled under N_2 by standard methods prior to use. Melting points were determined on an Electrothermal Mel-Temp apparatus and are uncorrected. Infrared spectra were obtained with a Bruker Tensor 27 spectrometer in the 4000–400 cm^{-1} spectral region as KBr disks. Combustion analyses were performed at the microanalytical laboratory of Instituto de Química. Electron Ionisation mass spectrometry (ESI MS) experiments were performed with a Bruker Daltonics Esquire 6000 spectrometer with ion trap. NMR spectra were recorded with a Bruker Avance III 400 or with a Bruker 300 with tetramethylsilane (TMS) as an internal standard. The ^{1}H–DOSY spectra were recorded at 25°C with 150 ms diffusion delay and 32 transients, using the 2D diffusion measurement Stimulated Echo & Led Bipolar Gradient (PFG–LED) with 2 spoil gradient ledgs2s pulse sequence in the standard Bruker pulse sequence library. Sample concentration of 10 mM was used to reduce viscosity changes and intermolecular interactions. Hydrodynamic radii in $CDCl_3$ were calculated by using the viscosity value $\eta CDCl_3$ = 0.542 × 10^{-3} $kg{\cdot}m^{-1}{\cdot}s^{-1}$, 298 K. Absorption spectra were obtained as MeOH solutions on a Unicam UV300 spectrometer using a deuterium lamp, whereas an Agilent UV-vis spectrophotometer model 8453 was employed to record the spectra as $CHCl_3$ solutions. All fluorescence spectra were recorded on a Fluorolog Horiba Spectrofluorometer equipped with a Xe lamp; the samples were excited at wavelength of absorption maxima λ_{max} = 280 nm, all emission measurements were carried out with 5 nm slit widths. Molecular modeling of macrocycles was performed with Merck Molecular Force Field (MMFF) methods on Spartan '08 software (Wavefunction, Irvine, CA). **Caution**: *Cadmium compounds should be handled with care due to their high toxicity. Metal perchlorates may undergo explosive reactions!*

M^{n+} Titration of L for $M_2L_2X_n$ formation and fluorescence enhancement studies

Methanolic solutions of **L** (2 mL, 8.5 × 10^{-6} M in MeOH) were prepared by repeated dilution, placed in a quartz cuvette and the initial fluorescence emission spectra were recorded. Small volumes (8.5–85 μL) of stock $ZnCl_2$, $Zn(ClO_4)_2$ and $AgSbF_6$ solutions (7.5 × 10^{-4} M in MeOH) were added sequentially to the cuvette using a microsyringe until maximum fluorescence intensity was observed, or a total volume of 4 mL was reached; the solutions were shaken well before recording measurements.

Fluorescence quenching study

2 mL stock solutions (8.5 × 10^{-6} M) of the selected macrocycles (**2**, **5**, **8** and **10**) in $CHCl_3$ was placed in a quartz cell of 1cm width and the quencher stock solution of picric acid (1.0 × 10^{-4} M) in $CHCl_3$ was added in incremental mode at room temperature; for titration measurements all macrocycles were excited at λ = 280 nm. The data were related as a Stern-Volmer plot of I_0/I against *[Q]*, and the association-quenching constants K_{ass} were calculated from the slope of the Stern-Volmer plot obtained by linear regression according to the equation:

$$I_o/I = 1 + K_{ass}[Q];$$

where I_o and I represent the fluorescence intensity before and after addition of quencher *Q*. Nevertheless, in the case of combined static and dynamic quenching, the Stern-Volmer plot exhibits an upward curve (concave toward the *y*-axis), the data were plotted as $[(I_o/I–1)/Q]$ versus $[Q]$, yielding a straight line with a slope of K_DK_S as K_{ass}, according to the following equation:[23]

$$I_o/I = 1 + K_{ass}[Q]$$

$$K_{ass} = [(I_o/I)–1][1/Q] = (K_D+K_S) + K_D+K_S[Q]$$

Synthesis of calix[4]arene L and $M_2L_2X_n$ metallomacrocycles 1-10

To prepare calix[4]arene **L**, we followed the procedure described below; in our hands, the reported method resulted in low and variable yields.[24]

{5,11,17,23-Tetra-tbutyl-25,27-dihydroxy-26,28-bis-(pyridine-4-ylmethoxy) calix[4]arene} (L). 5,11,17,23-tetra-*tert*-butyl-25,26,27,28-tetrahydroxy-calix[4]arene (1.00 g, 3.08 mmol) was dried under vacuum at 60°C for 1h whereupon anhydrous K_2CO_3 (4.26 g, 30.82 mmol) was added in CH_3CN (150 mL) and the mixture was refluxed for 2h under N_2 flow. Then, (4-chloromethyl)-pyridine hydrochloride (3.03 g, 18.49 mmol) and

Dalton Transactions Accepted Manuscript

KI (0.13 g, 0.77 mmol) were added and stirred for 2 h at 40°C, followed by reflux with vigorous stirring for 48 h. After this period, the reaction mixture was vacuum filtered and the solid was washed with hot MeCN; the mother liquor afforded a dark solid after solvent removal. This was dispersed and boiled in distilled water (250 mL) for 1 h, filtered, and washed thoroughly with hot water until the liquor was colourless. After column chromatography on silica gel with 20:1 CH_2Cl_2:MeOH as eluant, **L** was obtained as a colourless solid. Yield: 1.21 g (48%); m.p.: 109-111°C. IR (KBr): ν = 3391m (br) (O—H), [2955s, 2905w, 2866w] (C—H), [1602m, 1563w] (C═N), [1481s, 1460m, 1415m] (C═C), 1195s, 1019m, 804s. ^{1}H NMR (400 MHz, $CDCl_3$, 25°C): δ = 8.63 (d, $^3J_{H–H}$ = 6.0 Hz, 4H, Py), 7.64 (d, $^3J_{H–H}$ = 6.0 Hz, 4H, Py), 7.07 (s, 4H, Ar), 6.97 (s, 2H, OH), 6.79 (s, 4H, Ar), 5.07 (s, 4H, OCH_2–), 4.25 (d, $^2J_{H–H}$ = 13.1 Hz, 4H, –CH_2–), 3.33 (d, $^2J_{H–H}$ = 13.2 Hz, 4H, –CH_2–), 1.30 (s, 18H, ^{t}Bu), 0.93 (s, 18H, ^{t}Bu). ^{13}C NMR (75 MHz, $CDCl_3$, 25°C): δ = 150.6, 150.2, 149.5, 147.7, 146.3, 142.0, 132.4, 127.6, 125.8, 125.3, 121.4, 76.1, 34.0, 31.8, 31.7, 31.1. Elemental analysis calcd (%) for $C_{56}H_{68}N_2O_5$ C 79.21, H 8.07, N 3.30; found C 79.58, H 8.19, N 3.44.

All macrocycles were obtained through a similar protocol; preparation of macrocycle **1** is described below, while full detailed synthetic procedures for the rest of **1–10** macrocycles are provided in the Electronic Supplementary Information (ESI).

[$Zn_2L_2Cl_4$] (1). To a solution of zinc chloride (9.0 mg, 0.07 mmol) in acetonitrile was added **L** (50.1 mg, 0.06 mmol) in three portions under N_2 over 20 minutes. The resulting suspension was further stirred at room temperature for 4 h, the precipitate was vacuum filtered and washed with cold MeCN and cold MeOH to give **1** as a colourless solid. Yield: 52 mg, 91%; m.p.: 278-281°C. ^{1}H NMR (400 MHz, $CDCl_3$, 25°C): δ = 8.79 (br, 8H, Py), 8.01 (br, 8H, Py), 7.02 (s, 8H, Ar), 6.91 (br, 4H, OH), 6.76 (s {br}, 8H, Ar), 5.19 (s {br}, 8H, OCH_2–), 4.17 (d, $^2J_{H–H}$ = 13.0 Hz, 8H, –CH_2–), 3.30 (br, 8H, –CH_2–), 1.26 (s, 36H, ^{t}Bu), 0.92 (s {br}, 36H, ^{t}Bu). IR (KBr): ν = 3466m (br) (O—H), [2958s, 2867m] (C—H), 1622m (C═N), [1482s, 1431m] (C═C), 1259m, 1198s, 1028s, 795s. MS (+ESI, CH_3OH): m/z = 1897.8 [$Zn_2L_2Cl_4$–Cl^-]$^+$, 1798.9 [$Zn_2L_2Cl_4$–Zn^{2+}–$2Cl^-$+H^+]$^+$, 1761.9 [$Zn_2L_2Cl_4$–Zn^{2+}–$3Cl^-$]$^+$. Elemental analysis calcd (%) for $C_{112}H_{138}Cl_4N_4O_{11}Zn_2$ C 67.64, H 6.99, N 2.82; found C 67.51, H 6.76, N 2.80.

X ray diffraction of calix[4]arene L

A suitable single crystal of **L** was mounted on a glass fiber under cryogenic system and crystallographic data were collected with an Oxford Diffraction Gemini "A" diffractometer with a CCD area detector with $\lambda_{MoK\alpha}$ = 0.71073 Å and monochromator of graphite at 130 K. CrysAlisPro and CrysAlis RED software packages were used for data collection and integration.[25] The double pass method of scanning was used to exclude any noise. The collected frames were integrated by using an orientation matrix determined from the narrow frame scans. Final cell constants were determined by a global refinement; collected data were corrected for absorbance by using analytical numeric absorption correction using a multifaceted crystal model based on expressions upon the Laue symmetry using equivalent reflections.[26] Structure solution and refinement were carried out with the SHELXS-2014 and SHELXL-2014 packages;[27] WinGX v2014.1 software was used to prepare material for publication.[28] Full-matrix least-squares refinement was carried out by minimising $(Fo^2 – Fc^2)^2$. All non-hydrogen atoms were refined anisotropically. The H atom of the hydroxo group (H–O) was located in the difference map and refined isotropically with U_{iso}(H) = 1.5 for H–O. H atoms attached to C atoms were placed in geometrically idealized positions and refined as riding on their parent atoms, with C–H = 0.95–0.98 Å and with U_{iso}(H) = 1.2U_{eq}(C) for aromatic groups, and U_{iso}(H) = 1.5U_{eq}(C) for methyl groups. Crystal data and experimental details of the structure determination of **L** are listed in Table S1, ESI†. The crystallographic data for the structure reported in this paper has been deposited with the Cambridge Crystallographic Data Centre as supplementary publication no. CCDC 1403977. Copies of the data can be obtained free of charge on application to CCDC, 12 Union Road, Cambridge, CB2 1EZ, UK (fax: (+44) 1223-336-033, e-mail: deposit@ccdc.cam.ac.uk).

Acknowledgements

The authors thank L. Ríos, L. C. Márquez, and E. García for ESI MS, R. Patiño for IR spectroscopy, M. Orta for combustion analyses, and N. Esturau for DOSY NMR; EGP acknowledges DGAPA-UNAM for a post-doctoral fellowship. MV is grateful to the Swiss National Science Foundation for a post-doctoral fellowship.

Notes and references

1 (*a*) T. R. Cook and P. J. Stang, *Chem. Rev.,* 2015, DOI: 10.1021/cr5005666; (*b*) R. Chakrabarty, P. S. Mukherjee and P. J. Stang, *Chem. Rev.,* 2011, **111**, 6810–6918.

2 *For examples:* (*a*) Q-F. Sun, J. Iwasa, D. Ogawa, Y. Ishido, S. Sato, T. Ozeki, Y. Sei, K. Yamaguchi and M. Fujita, *Science,* 2010, **328**, 1144–1147; (*b*) Q.-F. Sun, S. Sato and M. Fujita, *Nature Chem.,* 2012, **4**, 330–333; (*c*) P. Mal, B. Breiner, K. Rissanen and J. R. Nitschke, *Science,* 2009, **324**, 1697–1699; (*d*) Y. K. Kryschenko, S. R. Seidel, A. M. Arif and P. J. Stang, *J. Am. Chem. Soc.,* 2003, **125**, 5193–5198; (*e*) M. Yamashina, T. Yuki, Y. Sei, M. Akita and M. Yoshizawa, *Chem. Eur. J.,* 2015, **21**, 4200–4204; (*f*) D. M. Wood, W. Meng, T. K. Ronson, A. R. Stefankiewicz, J. K. M. Sanders and J. R. Nitschke, *Angew. Chem. Int. Ed.,* 2015, **54**, 3988–3992; (g) N. Kishi, M. Akita and M. Yoshizawa, *Angew. Chem. Int. Ed.,* 2014, **53**, 3604–3607; (h) J.-P. Lang, Q.-F. Xu, Z.-N. Chen and B. F. Abrahams, *J. Am. Chem. Soc.*, 2003, **125**, 12682–12683; (i) D. Liu, J.-P. Lang and B. F. Abrahams, *J. Am. Chem. Soc.*, 2011, **133**, 11042–11045; (j) D. Liu, Z.-G. Ren, H.-X. Li, J.-P. Lang, N.-Y. Li and B. F. Abrahams, *Angew. Chem. Int. Ed.*,2010, **49**, 4767–4770; (k) P. S. Mukherjee, K. S. Min, A. M. Arif and P. J. Satng, *Inorg. Chem.*, 2004, **43**, 6345–6350.

3 (*a*) B. H. Northrop, H.-B. Yang and P. J. Stang, *Chem. Commun.,* 2008, 5896–5908; (*b*) B. H. Northrop, Y-R. Zheng, K.-W. Chi and P. J. Stang, *Acc. Chem. Res.,* 2009, **42**, 1554–1563; (*c*) V. Croué, S. Goeb and M. Sallé, *Chem. Commun.,* 2015, **51**, 7275–7289; (*d*) T. R. Cook, V. Vajpayee, M. H. Lee, P. J. Stang and K.-W. Chi, *Acc. Chem. Res.,* 2013, **46**, 2464–2474.

Dalton Transactions Accepted Manuscript

This journal is © The Royal Society of Chemistry 20xx

Please do not adjust margins

4 (*a*) L. Xu, Y.-X. Wang and H.-B. Yang, *Dalton Trans.,* 2015, **44**, 867–890; (*b*) J. A. Thomas, *Dalton Trans.,* 2011, **40**, 12005–12016; (*c*) A. Kumar, S.-S. Sun and A. J. Lees, *Coord. Chem. Rev.,* 2008, **252**, 922–939; (*d*) P. Thanasekaran, C.-H. Lee and K.-L. Lu, *Coord. Chem. Rev.,* 2014, **280**, 96–175.

5 X. Yan, T. R. Cook, P. Wang, F. Huang and P. J. Stang, *Nature Chem.,* 2015, **7**, 342–348.

6 (*a*) M.-L. He, S. Wu, J. He, Z. Abliz and L. Xu, *RSC Adv.,* 2014, **4**, 2605–2608; (*b*) L. Zhao, Y. Liu, C. He, J. Wang and C. Duan, *Dalton Trans.,* 2014, **43**, 335–343; (*c*) V. Vajpayee, Y. H. Song, M. H. Lee, H. Kim, M. Wang, P. J. Stang and K.-W. Chi, *Chem. Eur. J.,* 2011, **17**, 7837–7844.

7 (*a*) P. P. Neelakandan, A. Jiménez and J. R. Nitschke, *Chem. Sci.,* 2014, **5**, 908–915; (*b*) J. Wang, C. He, P. Wu, J. Wang and C. J. Duan, *J. Am. Chem. Soc.,* 2011, **133**, 12402–12405; (*c*) S. Shanmugaraju, K. B. Bar, H. Jadhav, D. Moon and P. S. Mukherjee, *Dalton Trans.,* 2013, **42**, 2998–3008. (*d*) S. Shanmugaraju, K. B. Bar, K.-W. Chi and P. S. Mukherjee, *Organometallics,* 2010, **29**, 2971–2980; (*e*) H. Ahmad, B. W. Hazel, A. J. H. M. Meijer, J. A. Thomas and K. A. Wilkinson, *Chem. Eur. J.,* 2013, **19**, 5081–5087.

8 J. W. Atwood, *Chem. Commun.,* 2013, **49**, 114–117.

9 *For example:* (*a*) S. Pasquale, S. Sattin, E. C. Escudero-Adán, M. Martínez-Belmonte and J. de Mendoza, *Nature Commun.* 2012, **3**, 785; (*b*) M. Liu, W. Liao, C. Hu, S. Du and H. Zhang, *Angew. Chem. Int. Ed.,* 2012, **51**, 1585–1588; (*c*) F. A. Cotton, P. Lei, C. Lin, C. A. Murillo, X. Wang, S.-Y. Yu and Z.-X. Zhang, *J. Am. Chem. Soc.,* 2004, **126**, 1518–1525.

10 (*a*) X.-F. Jiang, F. K.-W. Hau, Q.-F. Sun, S.-Y. Yu and V. W.-W. Yam, *J. Am. Chem. Soc.,* 2014, **136**, 10921–10929; (*b*) P. R. A. Webber, M. G. B. Drew, R. Hibbert and P. D. Beer, *Dalton Trans.,* 2004, 1127–1135.

11 *For examples:* (*a*) R. McLellan, M. A. Palacios, C. M. Beavers, S. J. Teat, S. Piligkos, E. K. Brechin and S. J. Dalgarno, *Chem. Eur. J.,* 2015, **21**, 2804–2812; (*b*) S. Wang, Y. Bi and W. Liao, *CrystEngComm,* 2015, **17**, 2896–2902; (*c*) K. Su, F. Jiang, J. Qian, Y. Gai, M. Wu, S. M. Bawaked, M. Mokhtar, S. A. Al-Thabaiti and M. Hong, *Cryst. Growth Des.,* 2014, **14**, 3116–3123.

12 (*a*) P. J. Stang, D. H. Cao, K. Chen, G. M. Gray, D. C. Muddiman and R. D. Smith, *J. Am. Chem. Soc.,* 1997, **119**, 5163–5168; (*b*) Z. Zhong, A. Ikeda, M. Ayabe, S. Shinkai, S. Sakamoto and K. Yamaguchi, *J. Org. Chem.,* 2001, **66**, 1002–1008.

13 F. Maharaj, R. Bishop, D. C. Craig, P. Jensen, M. L. Scudder and N. Kumar, *Cryst. Growth Des.,* 2009, **9**, 1334–1338.

14 (*a*) M. W. Cooke and G. S. Hanan, *Chem. Soc. Rev.,* 2007, **36**, 1466–1476; (*b*) M. W. Cooke, D. Chartrand and G. S. Hanan, *Coord. Chem. Rev.,* 2008, **252**, 903–921; (*c*) X.-J. Li, F.-L. Jiang, M.-Y. Wu, S.-Q. Zhang, Y.-F. Zhou and M.-C. Hong, *Inorg. Chem.,* 2012, **51**, 4116–4122.

15 (*a*) A. Castillo, J. L. Martínez, P. R. Martínez-Alanis and I. Castillo, *Inorg. Chim. Acta,* 2010, **363**, 1204–1211; (*b*) J. Olguín, A. Castillo, V. Gómez-Vidales, S. Hernández-Ortega, R. A. Toscano, E. Muñoz and I. Castillo, *Supramol. Chem*., 2009, **21**, 502–509.

16 (*a*) S. Chen, L.-J. Chen, H.-B. Yang, H. Tian, W. Zhu, *J. Am. Chem. Soc.,* 2012, **134**, 13596–13599; (*b*) L. Chen, Q. Chen, M. Wu, F. Jiang, M. Hong, *Acc. Chem. Res.,* 2015, **48**, 201–210; (*c*) N. W. Wu, J. Zhang, D. Ciren, Q. Han, L. J. Chen, L. Xu, H.-B. Yang, *Organometallics,* 2013, **32**, 2536–2545.

17 (*a*) L. Avram and Y. Cohen, *Chem. Soc. Rev.,* 2015, **44**, 586–602; (*b*) Z. Qi, T. Heinrich, S. Moorthy and C. A. Schalley, *Chem. Soc. Rev.,* 2015, **44**, 515–531.

18 (*a*) Y. Ding, Y. Tang, W. Zhu and Y. Xie, *Chem. Soc. Rev.,* 2015, **44**, 1101–1112; (*b*) G. M. Cockrell, G. Zhang, D. G. VanDerveer, R. P. Thummel and R. D. Hancock, *J. Am. Chem. Soc.,* 2008, **130**, 1420–1430; (*c*) Y.-H. Hsu, Y.-A. Chen, H.-W. Tsen, Z. Zhang, J.-Y. Shen, W.-T. Chuang, T.-C. Lin, C.-S. Lee, W.-Y. Hung, B.-C. Hong, S.-H. Liu and P.-T. Chou, *J. Am. Chem. Soc.,* 2014, **136**, 11805–11812; (*d*) S. Pal, N. Chatterjee and P. K. Bharadwaj, *RSC Adv.,* 2014, **4**, 26585–26620; (*e*) A. Y.-Y. Tam, K. M.-C. Wong and V. W.-W. Yam, *J. Am. Chem Soc.,* 2009, **131**, 6253–6260.

19 (*a*) J. W. Nugent, H. Lee, H.-S. Lee, J. H. Reibenspies and R. D. Hancock, *Inorg. Chem.,* 2014, **53**, 9014–9026; (*b*) J. W. Nugent, H. Lee, H.-S. Lee, J. H. Reibenspies and R. D. Hancock, *Chem. Commun.,* 2013, **49**, 9749–9751.

20 (*a*) Z. Li, N. Kishi, K. Yoza, M. Akita and M. Yoshizawa, *Chem. Eur. J.,* 2012, **18**, 8358–8365; (*b*) Z. Li, N. Kishi, K. Hasegawa, M. Akita and M. Yoshizawa, *Chem. Commun.,* 2011, **47**, 8605–8607.

21 (*a*) S. Shanmugaraju and P. S. Mukherjee, *Chem. Eur. J.,* 2015, **21**, 6656–6666; (*b*) D. Samanta, and P. S. Mukherjee, *Dalton Trans.,* 2013, **42**, 16784–16795; (*c*) M. Wang, V. Vajpayee, S. Shanmugaraju, Y.-R. Zeng, Z. Zhao, H. Kim, P. S. Mukherjee, K.-W. Chi and P. J. Stang, *Inorg. Chem.,* 2011, **50**, 1506–1512; (*d*) A. Chowdhury and P. S. Mukherjee, *J. Org. Chem.*, 2015, **8**, 4064–4075; (e) M.-M. Chen, X. Zhou, H. X. Li and J.-P. Lang, *Cryst. Growth Des*., 2015, **15**, 2753–2760; (f) S. Ghosh and P. S. Mukherjee, *Organometallics*, 2008, **27**, 316–319.

22 S. Shanmugaraju, S. A. Joshi and P. S. Mukherjee, *Inorg. Chem.,* 2011, **50**, 11736–11745.

23 J. R. Lakowicz, *Principles of Fluorescence Spectroscopy*, Springer, 2006.

24 I. I. Stoikov, L. I. Gafiullina, D. Sh. Ibragimova, I. S. Antipin and A. I. Konovalov, *Russ. Chem. Bull., Int. Ed.,* 2004, **53**, 1172–1180.

25 Agilent (2013). *CrysAlis PRO* and *CrysAlis RED*. Agilent Technologies, Yarnton, England.

26 R. C. Clark and J. S. Reid, *Acta Cryst*., 1995, **A51**, 887–897.

27 G. M. Sheldrick, *Acta Cryst.*, Sect. A: Found. Crystallogr., 2008, 64, 112-122.

28 L. J. Farrugia, *Appl. Cryst.,* 1999, **32**, 837–838.

Dalton Transactions Accepted Manuscript

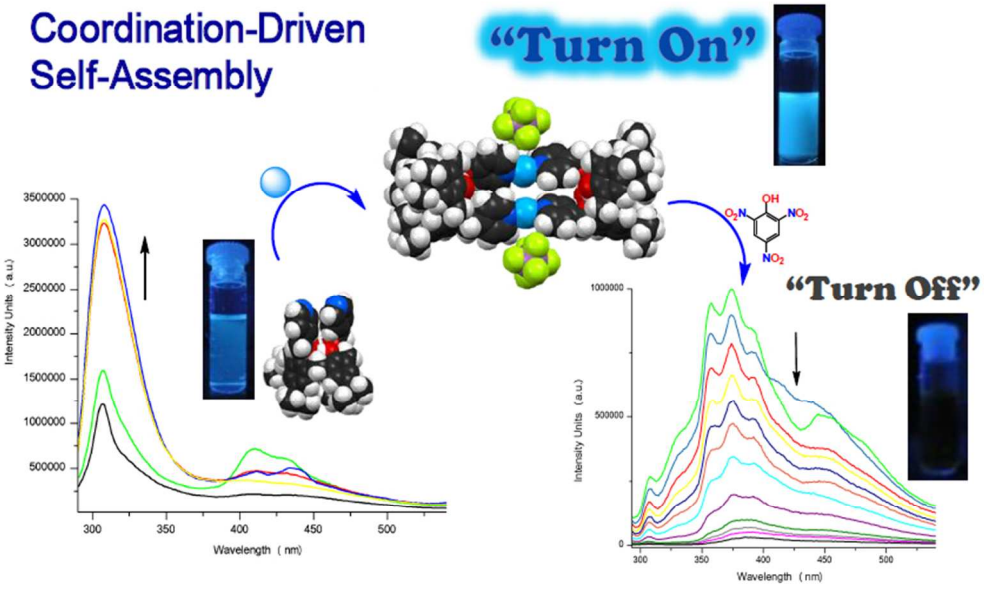

Photoactive calixarene-based metallamacrocycles $\mathbf{M_2L_2X_n}$ are obtained through coordination-driven self-assembly between semi-flexible calixarene **L** and Zn^{2+}, Pd^{2+}, Ag^{+}, and Cd^{2+}. Blue emission enhancement of **L** up to 13-fold is observed upon assembly, likely due to increased rigidity. $\mathbf{M_2L_2X_n}$ act as turn-off sensors with picric acid as emission quencher.
225x141mm (96 x 96 DPI)

Dalton Transactions Accepted Manuscript